Author(s): Christoph Ungemach, Neil Stewart and Stian Reimers

Article Title: Domain variance and superstructure across the antiferroelectric/ferroelectric phase boundary in Pb1−1.5xLax (Zr0.9Ti0.1)O3
Year of publication: 2003
Link to published article: http://dx.doi.org/10.1557/JMR.2003.0037

Domain variance and superstructure across the antiferroelectric/ferroelectric phase boundary in $Pb_{1-1.5x}La_x(Zr_{0.9}Ti_{0.1})O_3$

Jesper Knudsen, D.I. Woodward, and Ian M. Reaney
Department of Engineering Materials, Sir Robert Hadfield Building, University of Sheffield, Mappin St., Sheffield S1 3JD, United Kingdom

(Received 31 July 2002; accepted 14 October 2002)

Transmission electron microscopy, x-ray diffraction, relative permittivity as a function of temperature, and polarization versus field loops were used to study the antiferroelectric/ferroelectric (AFE/FE) phase boundary in $Pb_{1-1.5x}La_xZr_{0.9}Ti_{0.1}O_3$ (PLZT, 100*x*/90/10) ceramics. X-ray diffraction and electrical measurements indicated a FE rhombohedral (R) to AFE tetragonal (T) phase transition between PLZT 2/90/10 and 4/90/10. Both phases exhibited superstructure reflections in electron-diffraction patterns at $\frac{1}{2}\{hkl\}$ positions consistent with rotations of the octahedra in antiphase. Previously, neutron diffraction suggested that the FE_R has an $a^-a^-a^-$ tilt system (Glazer notation), in agreement with its macroscopic symmetry. By analogy, it is proposed that the AFE_T phase has an $a^0a^0c^-$ tilt system. The AFE phase was also characterized by incommensurate superstructure along pseudocubic $\langle 110\rangle_p$ directions, whereas the FE phase had extra commensurate superlattice reflections at $\frac{1}{2}\{hk0\}_p$ positions. $\frac{1}{2}\{hk0\}_p$ reflections are forbidden in both tilt systems, but their presence is explained by Pb ion displacements averaged along $\langle 111\rangle$ but with short coherence antiparallel components along $\langle 110\rangle$ directions. The antiparallel Pb displacements are coupled to an $a^-b^-b^-$ ($a \approx b$) monoclinic tilt system in the vicinity of the AFE/FE boundary.

I. INTRODUCTION

In the $PbZrO_3$–$PbTiO_3$ (PZT) solid solution, an antiferroelectric/ferroelectric (AFE/FE) phase boundary exists at Zr:Ti ratio approximately 96/4 (abbreviated PZT 96/4). At this boundary, switching from the AFE to the FE state using an applied field or stress induces large effective strains or charges. Commercial compositions are often doped with La, Nb, or Sn to broaden the phase transition and reduce the free energy difference between the AFE and FE phases.[1,2] Doping with La generally increases the stability of the AFE phase with respect to FE. The phase diagram for this system, shown in Fig. 1, was first reported by Haertling and Land in 1971.[3] The stabilization of the AFE state in La-doped PZT has been attributed to a disruption of the long-range dipolar interaction, suppressing the FE state, which has less effect on the AFE state at low La contents. At high La contents (>4 at.%), the disruption is sufficient to additionally destabilize the AFE state resulting in the onset of "relaxor" behavior.[4]

The AFE phase in PLZT, commonly used for commercial compositions, has been ascribed a tetragonal (AFE_T) rather than orthorhombic (AFE_O) structure.[5–7] Recent work, however, has suggested that it is incommensurate ($AFE_{T/In}$) with no unique crystal symmetry.[8–10] Instead, it contains a structural modulation parallel with some $\langle 110\rangle_p$ directions. (Note: subscript "p" indicates a pseudocubic structure.)

From electron diffraction studies, it has been suggested that the AFE/FE phase transition in pure PZT is accompanied by a transformation from antiphase to in-phase rotations of O-octahedra.[11–13] The latter structural distortion was considered by the authors of Refs. 11 and 12 to give rise to $\frac{1}{2}\{hk0\}$ reflections in the FE phase. However, to date, no structural refinement of neutron diffraction data has confirmed this hypothesis and only antiphase rotations have been found.[14] Therefore, PZT 90/10 has been ascribed an $a^-a^-a^-$ octahedral tilt system, according to the Glazer notation,[15–17] consistent with the rhombohedral FE distortion ($R3c$). The tilt system(s) in La-doped PZT is/are unknown.

In this investigation, macroscopic changes in structure and properties of $Pb_{1-1.5x}La_xZ_{0.9}Ti_{0.1}O_3$ (PLZT 100*x*/90/10) are studied using x-ray diffraction (XRD), relative permittivity (ϵ_r) versus temperature plots, and polarization versus field loops. Transmission electron microscopy (TEM) is used to investigate planar defects and domain variance associated with superlattice reflections.

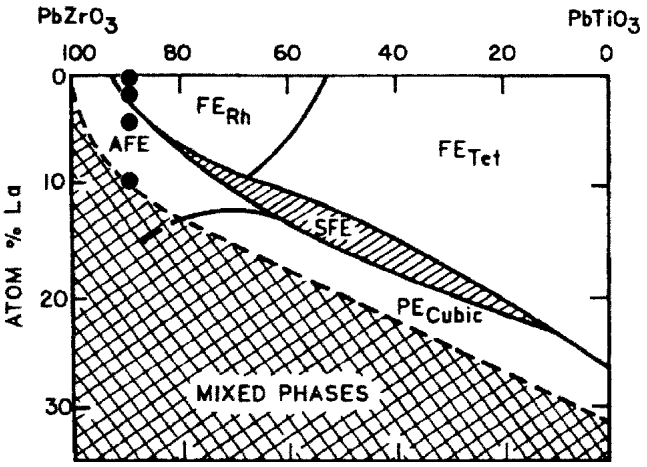

FIG. 1. PLZT phase diagram, after Haertling and Land.[3] Points indicate the compositions fabricated, PLZT 100*x*/90/10 (100*x* = 0, 2, 4, and 10). AFE = antiferroelectric, FE_{Rh} = ferroelectric rhombohedral, FE_{Tet} = ferroelectric tetragonal, SFE = slim-loop ferroelectric, and PE_{Cubic} = paraelectric cubic.

II. EXPERIMENTAL

A. Sample preparation

PLZT 100*x*/90/10 samples with 100*x* = 0, 2, 4, and 10 were prepared by a conventional mixed oxide route using standard laboratory reagent grade starting powders (>99.9% purity). The La raw material was calcined for 2 h at 1000 °C and checked by XRD to ensure that pure La_2O_3 was present before batching. The raw materials were mixed with 5 wt% excess PbO to act as a sintering aid and to compensate for the lead loss during sintering. Calcination was typically carried out at 850 °C for 6 h in a lidded alumina crucible, followed by crushing and sieving. The calcined powder was then attrition milled at 400 rpm for 1½ h with 2 wt% poly(ethylene glycol) (PEG, grade 10,000) binder added, dried, reground, and sieved. Submicron particle sized powders, $d_{mean} \approx 0.6–0.8$ μm, measured on a LS130 Coulter laser particle sizing device, were obtained through this route.

Pellets were uniaxial cold pressed in a steel die, embedded, and fully covered in granulated PZ powder and sintered at 1250 °C for 3 h in air in a lidded alumina boat to ensure a lead-rich atmosphere during sintering. Samples routinely achieved densities greater than 95% of theoretical.

B. X-ray diffraction

Pellets were ground to a fine powder and sprinkled onto an acetate foil covered with vacuum grease. The foil was placed in a circular sample holder, which was rotated. XRD data were collected on a STOE STADI P (Darmstadt, Germany) diffractometer using Cu $K_{\alpha 1}$ radiation (λ = 1.540562 Å), a scanning range of 10–95° in 2θ, a scanning speed of 2°/min, and 0.02° in 2θ step size. Sietronics XRD Trace Processing software (Belconnen, Australia) and STOE WinXPOW software (Darmstadt, Germany) were used to identify the peaks and phases present.

C. Transmission electron microscopy

TEM specimens were prepared by mounting a pellet onto a glass slide with thermosensitive resin and grinding to approximately 20–30 μm. The 3.05-mm Cu support rings with a 1000-μm hole were glued on to the disc, and excess material was chipped away from the ring edges using a razor blade. A Gatan (Pleasanton, CA) dual ion mill, operating at 6 kV, a total beam current of 0.6 mA, and at an incidence angle of 15° was used to thin the specimen to electron transparency. Samples were examined using JEOL 3010 (300 kV) (Tokyo, Japan) and Philips TECNAI (200 kV) (Eindhoven, The Netherlands) TEM microscopes.

D. Electrical measurements

Low-field, relative permittivity (ϵ_r) as a function of temperature was measured at 1 kHz fixed frequency on a Hewlett Packard 4284A (Palo Alto, CA) Precision LCR-meter operating in conjunction with a computer-controlled furnace. Before measurement, each pellet surface was polished to eliminate any surface roughness or Pb deficiency encountered during sintering. Sputtered gold electrodes were then applied.

High-field polarization versus electric field (PE) hysteresis experiments were performed at room temperature under silicone oil using a computer-controlled generator, HP 33120A (Hewlett Packard, Palo Alto, CA), and a high-voltage amplifier, Trek 609D-6 (Trekinc, Medina, NY). A current amplifier, Stanford Research Systems model SR570 (Sunnyvale, CA), was used to measure the induced current, which was then integrated numerically to obtain the charge *Q* and thus the polarization *P*. The applied field and induced current were downloaded to the computer using a Tektronix TDS 420 DSO (Bracknell, United Kingdom). Ceramic pellets were ground to thin discs (approximately 0.6–0.7-mm thickness), which were representative of the bulk. Gold pasted electrodes were applied and fired-on at 800 °C. A frequency of 10 Hz was used for all samples with a maximum voltage of 4 kV.

III. RESULTS AND DISCUSSION

A. XRD, relative permittivity, and ferroelectric hysteresis

Figure 2 shows the XRD patterns from PLZT 100*x*/90/10 where 100*x* = 0, 2, 4, and 10. PZT 90/10 and PLZT 2/90/10 show splitting of the $(111)_p$ peak, indicating a rhombohedral structure, although the latter exhibits only a shoulder, suggesting that the rhombohedral distortion decreases with increasing La content. In PLZT 4/90/10 and 10/90/10, the $(200)_p$ rather than $(111)_p$ peak

is split, indicating a tetragonal distortion of the cation sublattice. Once again however, the distortion decreases with increasing La concentration. Relative permittivity versus temperature plots for all compositions on both heating and cooling at 2°/min are shown in Fig. 3. A decrease in T_c from 255 to 198 °C occurs (cooling curve) as La concentration increases from 0/90/10 to 2/90/10 but without a significant change in the magnitude of the permittivity maximum (approximately 23,000). Further decreases together with broadening of T_c are observed for PLZT 4/90/10 and PLZT 10/90/10 accompanied by a reduction in relative permittivity (approximately 1000). Figure 4 shows the PE hysteresis loops for PLZT 100*x*/90/10. For $x = 0$ and 2, a classic square FE hysteresis loop is obtained whereas for $x = 4$ and 10 the sample behaves as a linear dielectric, characteristic of a nonswitching AFE phase. The abrupt decrease in relative permittivity and the change in PE curve from classic FE to linear dielectric between PLZT 2/90/10 and PLZT 4/90/10 supports the XRD data that a structural phase boundary is present between these two compositions, as suggested by Haertling and Land.[3]

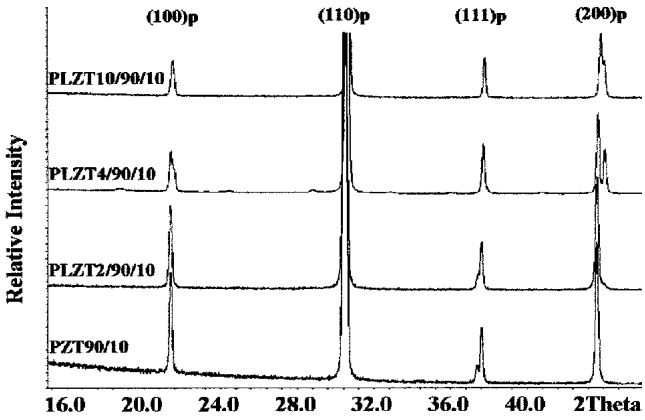

FIG. 2. XRD patterns of PLZT 100*x*/90/10 ($100x = 0$, 2, 4, and 10). $(111)_p$ peak splitting indicates a rhombohedral distortion for PZT 90/10 and PLZT 2/90/10. $(200)_p$ peak splitting indicates a tetragonal distortion for PLZT 4/90/10 and PLZT 10/90/10.

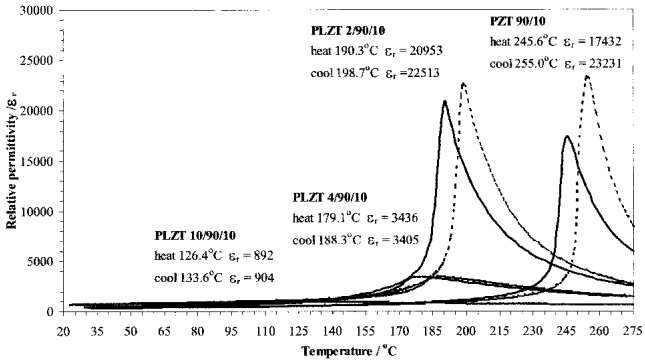

FIG. 3. ϵ_r versus temperature plots for PLZT 100*x*/90/10 ($100x = 0$, 2, 4, and 10) on cooling. Temperatures at ϵ_r(max) for all compositions are indicated.

B. Transmission electron microscopy

1. PZT 90/10

The structural changes that occur between PZ and PZT 85/15 have been discussed by the authors of Refs. 4, 14, 15, 18, and 19. However, there is no consensus explanation for the observed changes in superlattice reflections across the AFE/FE phase boundary. Dai *et al.*[12] have suggested that there is a switch from antiphase to inphase tilting across the AFE/FE boundary which results in the replacement of $\frac{1}{2}\{hkl\}_p$ with $\frac{1}{2}\{hk0\}_p$ superlattice reflections. Ricote *et al.*,[14] in agreement with earlier work on PZ–$BaTiO_3$ compositions by Reaney *et al.*,[18] refute this argument claiming that the $\frac{1}{2}\{hk0\}_p$ superlattice reflections observed in the FE phase arise from cation displacements and not inphase tilting. More recently, Watanabe and Koyama[19] have discussed the presence of an incommensurate phase related to an M-point condensation of a soft mode (Glazer[16]), associated with in-phase tilting.

Despite these contradictory interpretations, the type of domain structure and variance observed by each set of authors is identical. Here, the domain structure associated with La-doped PZT 90/10 is under investigation rather than PZT 95/5. However, for PZT 90/10, the superlattice reflections discussed by the above authors are too weak to image. Therefore a PZT 95/5 composition has also been studied. It is assumed that the source of the superlattice reflections in PZT 95/5 are the same and that any domain variance is consistent with PZT 90/10.

Figure 5(a) shows a bright-field (BF) TEM image of a typical domain structure observed in PZT 90/10. Figure 5(b) is a $[0\bar{1}1]_p$ zone axis diffraction pattern (ZADP) from a grain similar to that in Fig. 5(a). The strong reflections are indexed according to the simple perovskite lattice, and two distinct types of weak superlattice reflections are observed at $\frac{1}{2}\{hkl\}_p$ and $\frac{1}{2}\{0kl\}_p$. The space group for this composition has been determined by x-ray and neutron diffraction as $R3c$.[14,15] It is a doubled unit cell with a rhombohedral distortion in which the O lattice may be described by the tilt system $a^-a^-a^-$, according to Glazer.[15] For this tilt system, reflections at the $\frac{1}{2}\{hkl\}_p$ positions where either $h \neq k$, $k \neq l$, or $h \neq l$ are allowed. The lowest order reflections permitted are therefore $(\frac{3}{2}\frac{1}{2}\frac{1}{2})_p$. In Fig. 5(b), however, weak reflections are clearly present at $(\frac{1}{2}\frac{1}{2}\frac{1}{2})_p$, forbidden according to the tilt system. This contradiction may be rationalized by considering that dynamical conditions apply to electron scattering, permitting the double diffraction route,

$$\{\tfrac{3}{2}\tfrac{1}{2}\tfrac{1}{2}\}_p + \{\bar{1}00\}_p = \{\tfrac{1}{2}\tfrac{1}{2}\tfrac{1}{2}\}_p \quad .$$

It is concluded therefore that this composition contains antiphase tilting, consistent with an $a^-a^-a^-$ space group, in agreement with x-ray and neutron diffraction.[14,15]

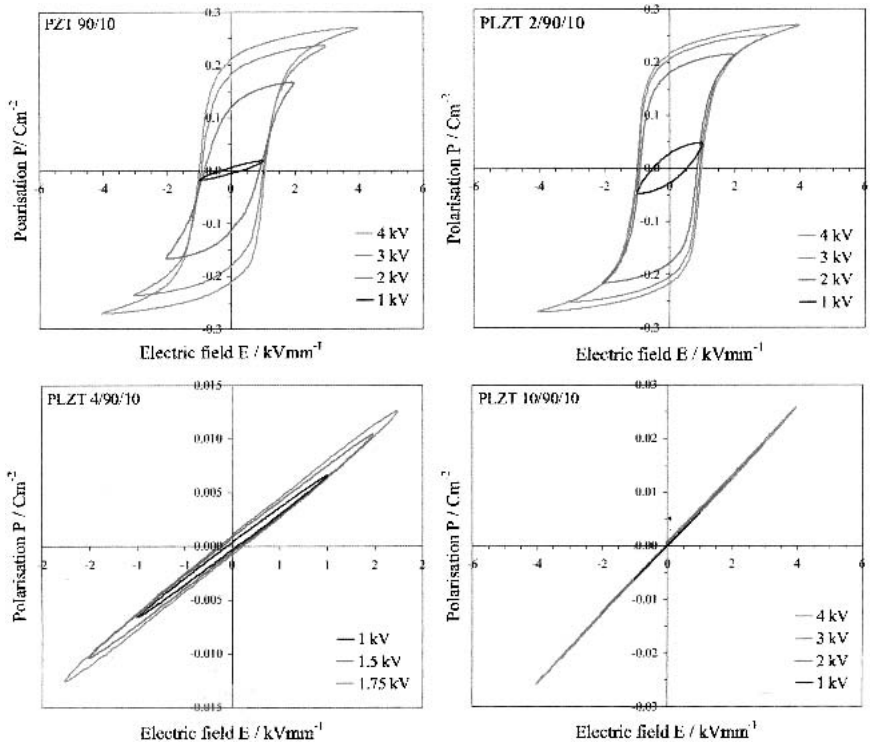

FIG. 4. Polarization versus field loops for PLZT 100*x*/90/10, where $100x = 0$, 2, 4, and 10.

Reflections at the $\frac{1}{2}\{0kl\}_p$ positions, also observed in Fig. 5(b), are also forbidden in the $a^-a^-a^-$ tilt system. It has been postulated by Dai *et al.*[11,12] and Watanabe and Koyama[19] that these reflections arise from inphase rotations of the O-octahedra. However, according to Glazer,[15,16] the lowest ordered reflections allowed by inphase tilting are $\{\frac{3}{2}\frac{1}{2}0\}_p$. This reflection is not allowed by the zone law in any $\langle 110\rangle_p$ zone axes where h must always equal k in magnitude, i.e.,

$$h \times U + k \times V + l \times W = 0 \quad ,$$
$$\tfrac{3}{2} \times \bar{1} + \tfrac{1}{2} \times 1 + 0 \times 0 \neq 0 \quad ,$$
$$\tfrac{1}{2} \times \bar{1} + \tfrac{1}{2} \times 1 + 0 \times 0 = 0 \quad .$$

If these reflections arise from inphase tilting of O-octahedra, either the original calculations of Glazer[15,16] are incorrect or there is a route for double diffraction. Extensive investigations of systems that contain inphase tilting, e.g., $CaTiO_3$,[16,20] would indicate that Glazer's original calculations are correct and, furthermore, no route for double diffraction exists in the $\langle 110\rangle$ zone axes for simple perovskites.[21]

There are two potential sources of superlattice reflections other than octahedral rotations in stoichiometric perovskites, ordering of different cation species and antiparallel displacements of cations.[21] Members of the PZT solid solution have been structurally refined many times, and there is no evidence of cation ordering. It is therefore an unlikely source of superlattice. Thus, by elimination, the superlattice reflections at $\frac{1}{2}\{hk0\}_p$ must arise from antiparallel cation displacements. This conclusion agrees with the work of Ricote *et al.*[14] and earlier work by Reaney *et al.*[18] on PZ–$BaTiO_3$.

The reflections in Fig. 5(b) are too weak to be imaged reliably in dark field (DF). Therefore, as discussed previously, a PZT 95/5 sample was examined which exhibited more intense $\frac{1}{2}\{hk0\}_p$ superlattice reflections. Figure 6 is a DF image obtained using a $\frac{1}{2}\{hk0\}_p$ reflection with the electron beam parallel with the $\langle 111\rangle_p$ zone axis. Hairpin-shaped antiphase boundaries (APB) are present along with isolated APBs. These results are identical to those observed by Watanabe and Koyama,[19] Ricote *et al.*,[14] and earlier work on PZ–$BaTiO_3$ by Reaney *et al.*[18] Furthermore, $\frac{1}{2}\{hk0\}_p$ superlattice reflections of this nature have been observed in $Pb(Sc_{1/2}Ta_{1/2})O_3$ by Randall *et al.*[22] which give rise to bright regions in DF images when the sample is cooled to −100 °C. Reaney *et al.*[18] and Watanabe and Koyama[19] reported domain variance of the superlattice reflections with $\{hk0\}_p$, $\{h0l\}_p$, and $\frac{1}{2}\{0kl\}_p$, illuminating different regions. The macroscopic symmetry as determined by x-ray and neutron diffraction is *R*3*c*. The domain variance observed in the superlattice reflections suggests that locally the symmetry is lower.

The origin of the $\frac{1}{2}\{hk0\}_p$ reflections at the AFE–FE phase boundary in the PZT phase diagram is clearly controversial. So far, none of these reflections have been

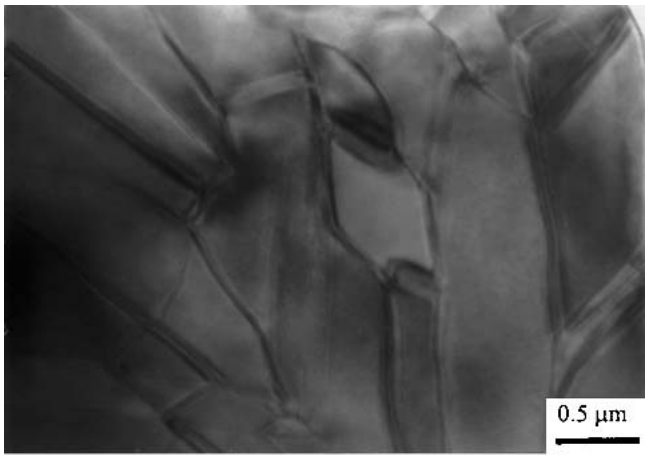

(a)

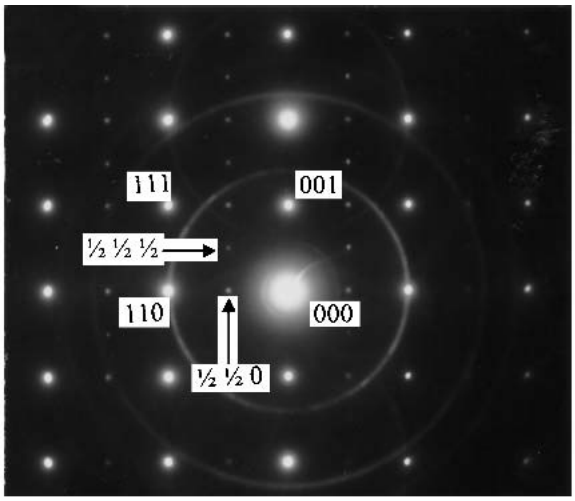

(b)

FIG. 5. (a) BF TEM image of the domain structure in a grain of PZT 90/10. (b) $[0\bar{1}1]_p$ zone axis electron diffraction pattern (ZADP) showing $½\{hk0\}_p$ and $½\{hkl\}_p$ superlattice reflections typical of the FE phase.

observed by x-ray or neutron diffraction and Ricote *et al.*[14] have suggested that the superlattice is stabilized by the large surface area/volume ratio in TEM samples. However, the concept of in-phase rotational displacements (tilting) giving rise to $½\{hk0\}_p$ reflections, as suggested by Dai *et al.*[11–13] and Watanabe and Koyama,[19] is flawed unless an explanation can be found for their presence in $\langle 110\rangle_p$ zones. It is more likely that they arise from cation displacements for which the condition $h \neq k$ in magnitude does not apply (Sec. IV).

2. PLZT 2/90/10

XRD, permittivity, and PE measurements (Figs. 2–4) suggest PLZT 2/90/10 is rhombohedral and FE, consistent with the phase diagram of Haertling and Land.[3] Figures 7 and 8 show a BF TEM image and the associated $\langle 111\rangle_p$ ZADPs, respectively, from this composition.

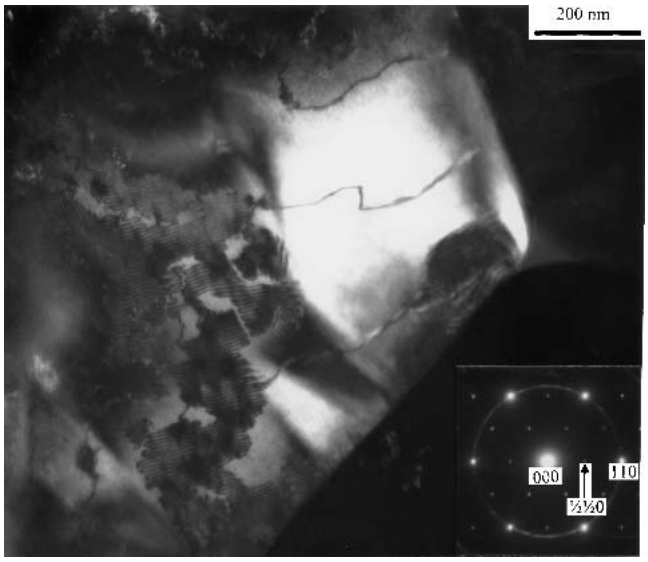

FIG. 6. DF TEM image of a grain in PZT 95/5 obtained using the $½\{hk0\}_p$ superlattice reflection indicated in the inset $\langle 111\rangle_p$ ZADP.

A complex modulated domain structure is observed in the majority of the grain (A), but nonmodulated regions are also present (B). The modulated domain structure gives rise to weak $½\{hk0\}_p$ superlattice reflections in the $\langle 111\rangle_p$ ZADP associated with the FE rhombohedral phase,[18] while nonmodulated domains exhibit incommensurate streaking along $\langle 110\rangle_p$ typical of the $AFE_{T/In}$ phase discussed by Xu *et al.*[8–10] and Reaney *et al.*[18]

Macroscopically, PLZT 2/90/10 behavior is dominated by the FE phase, which is present in most grains. This gives rise to a large permittivity maximum typical of a polar phase transition. However, there is inevitably a distribution of La^{3+} within the sample and some regions will have sufficient on the A site to stabilize the $AFE_{T/In}$ phase. This heterogeneity even occurs within grains which often demonstrate the coexistence of $AFE_{T/In}$ and FE regions. The FE regions are identified by the $½\{hk0\}_p$ reflections discussed extensively in Sec. III. B. 1. Their disappearance in the $AFE_{T/In}$ has been previously observed in Sn- and Ba-doped compositions by Xu *et al.*[8] and Reaney *et al.*[18]

3. PLZT 4/90/10

In agreement with the phase diagram of Haertling and Land,[3] XRD, permittivity, and PE measurements (Figs. 2–4) confirm that PLZT 4/90/10 is tetragonal and AFE. Furthermore, $\langle 111\rangle_p$ and $\langle 001\rangle_p$ zone axis electron-diffraction patterns frequently reveal an incommensurate modulation similar to that in Fig. 8.

Figures 9 and 10 show a BF TEM image and the associated $\langle 110\rangle_p$ ZADPs, respectively, of a typical grain in PLZT 4/90/10. The $\langle 110\rangle_p$ ZADPs have been recorded from alternate domains within the grain shown in Fig. 9.

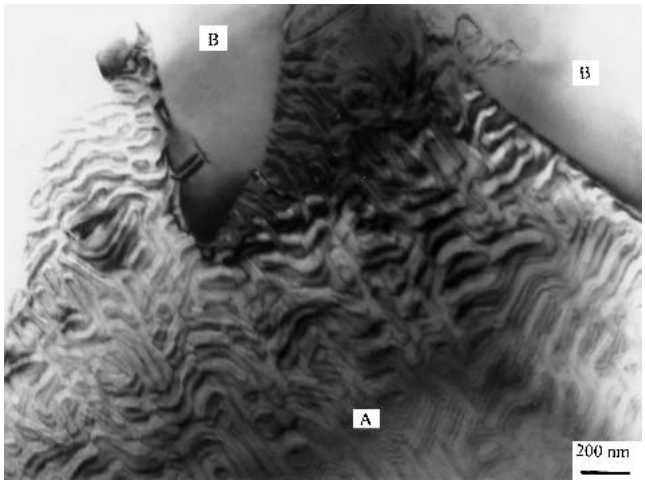

FIG. 7. BF TEM image showing (A) modulated and (B) nonmodulated domain structure in a grain of PLZT 2/90/10.

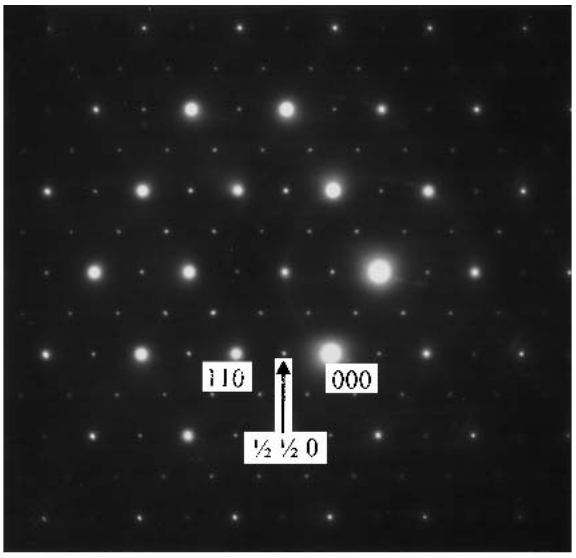

(a)

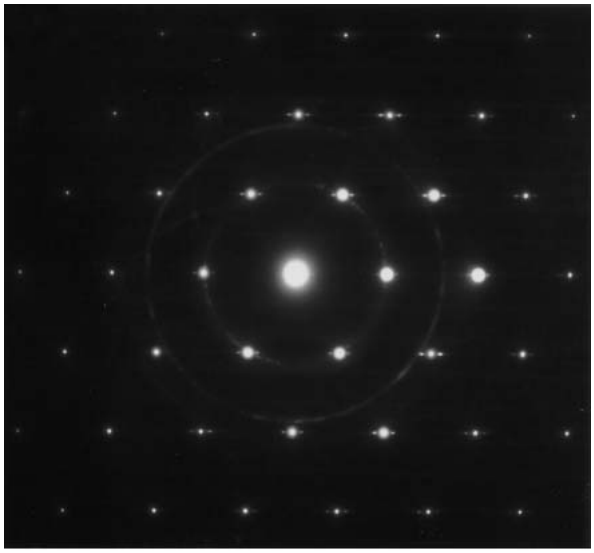

(b)

FIG. 8. $\langle 111 \rangle_p$ ZADPs associated with Fig. 6 for (a) modulated domain structure showing $\frac{1}{2}\{hk0\}_p$ superlattice reflections and (b) nonmodulated domain structure exhibiting incommensurate streaking and reflections along the [110] direction.

Strong discrete $\frac{1}{2}\{hkl\}_p$ superlattice reflections arise from some domains, whereas adjacent domains do not show these spots even after long exposure times (50 s). $\frac{1}{2}\{hkl\}_p$ reflections result from rotations of the octahedra in antiphase and are given a "-ve" superscript in the Glazer notation.[15,16] Structural refinements of the PZT 90/10 have determined the presence of an $a^-a^-a^-$ tilt system consistent with the rhombohedral FE distortion.[14] In the $a^-a^-a^-$ tilt system, electron-diffraction simulations suggest that $\frac{1}{2}\{hkl\}_p$ reflections appear in $\frac{6}{12}$ of $\langle 110 \rangle_p$ zone axes. Although axes are tilted in antiphase and all $\frac{1}{2}\{hkl\}_p$ could theoretically occur, 50% are absent due to symmetry considerations; i.e., all tilt angles are equal giving a net rotation around $\langle 111 \rangle_p$. For the tilt systems $a^0a^0c^-$ (one axis tilted in antiphase) and $a^0b^-b^-$ (two axes tilted in antiphase with equivalent amplitudes), electron-diffraction simulations suggest that $\frac{8}{12}$ and $\frac{10}{12}$ $\langle 110 \rangle_p$ directions contain $\frac{1}{2}\{hkl\}_p$ spots, respectively. Therefore, it is difficult to ascribe unambiguously a tilt system based uniquely on the domain variance of the $\langle 110 \rangle_p$ directions, except by the statistical analysis of several tens of domains. However, Glazer[16] suggests that the tilt system present in a perovskite reflects its macroscopic symmetry. Hence, it is proposed that the tilt system for PLZT 4/90/10 is tetragonal and gives rise to $\frac{1}{2}\{hkl\}_p$ reflections. Only $a^0a^0c^-$ of the systems described by Glazer satisfies this criteria. The domain variance of the superlattice (Figs. 9 and 10) is consistent with but does not confirm this premise, but it should be noted that refinement of neutron-diffraction data recently performed by Corker *et al.* (1997)[23] reported an $a^0b^-b^-$ tilt system for PZ. This tilt system gives rise to an orthorhombic oxygen sublattice consistent with the orthorhombic cation sublattice described by the antiparallel Pb displacements.

4. PLZT 10/90/10

In agreement with the phase diagram of Haertling and Land,[3] XRD, permittivity, and PE measurements (Figs. 2–4) suggest that PLZT 10/90/10 is $AFE_{T/In}$. A BF TEM image and $\langle 100 \rangle_p$ ZADPs of PLZT 10/90/10 are shown in Figs. 11 and 12, respectively. Domains, alternately featureless and containing a bright and dark "patchwork" of contrast, are observed. Incommensurate satellite reflections and streaking along $\langle 110 \rangle_p$ directions appear in $\langle 100 \rangle_p$ diffraction patterns recorded from the patchwork domain structure but not from featureless domains. Two explanations are possible; first, the domains

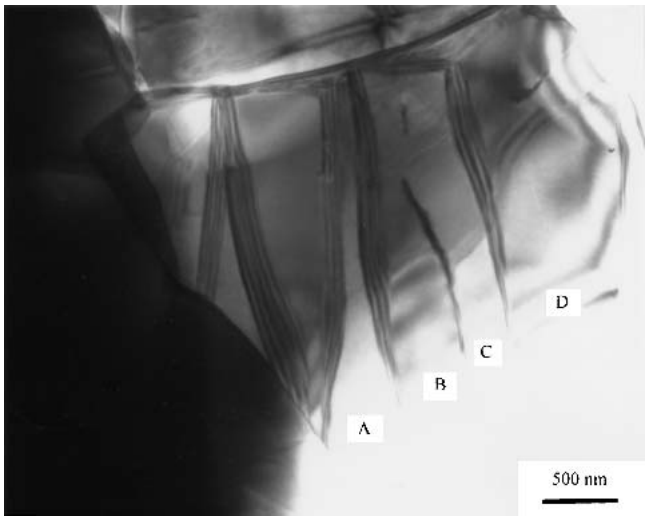

FIG. 9. BF TEM image showing the domain structure in a grain of PLZT 4/90/10.

represent regions which are alternately paraelectric and $AFE_{T/In}$. The former phase would not give rise to superstructure in diffracted images. The second and, in our view more likely explanation, is that the incommensurate modulation occurs in 2D only (e.g., in the *a*, *b* plane of the perovskite cell) and that perpendicular to this plane (i.e., parallel to a $[001]_p$ rather than $[100]_p$ or $[010]_p$ zone axis) the incommensurate reflections are forbidden.

Figure 8 (PLZT 2/90/10) shows a modulated superstructure identical to that observed in Fig. 12 except the incommensurate reflections are elucidated in $\langle 111\rangle_p$ rather than $\langle 001\rangle_p$ zone axes. In Fig. 8, the fundamental reflections are indexed according to a simple perovskite lattice and the spots nearest to 000 are $(hk0)_p$, $(h0l)_p$, and $(0kl)_p$. It is clear therefore that the incommensurate modulation only occurs along $[hk0]_p$ directions and not along $[h0l]_p$ and $[0kl]_p$. If this crystallographic information is adapted for $\langle 001\rangle_p$ zone axes, an incommensurate modulation may only be observed according to the zone law in $[001]_p$ and not in $[100]_p$ and $[010]_p$ directions. The origin of the patchwork contrast, however, remains to be elucidated.

IV. DISCUSSION

The domain structure in PLZT (100*x*/90/10) shows distinct changes as a function of *x*. From $100x = 0 \rightarrow 2$, a rhombohedral FE phase dominates with superlattice reflections at $\frac{1}{2}\{hkl\}_p$ positions associated with octahedral rotations in antiphase, consistent with an *R*3*c* space group. In addition, $\frac{1}{2}\{hk0\}_p$ reflections, forbidden according to the macroscopic symmetry, are also present. Without neutron/x-ray data any structural model which explains the reflections is, by definition, speculation. However, the TEM observations are irrefutable and the

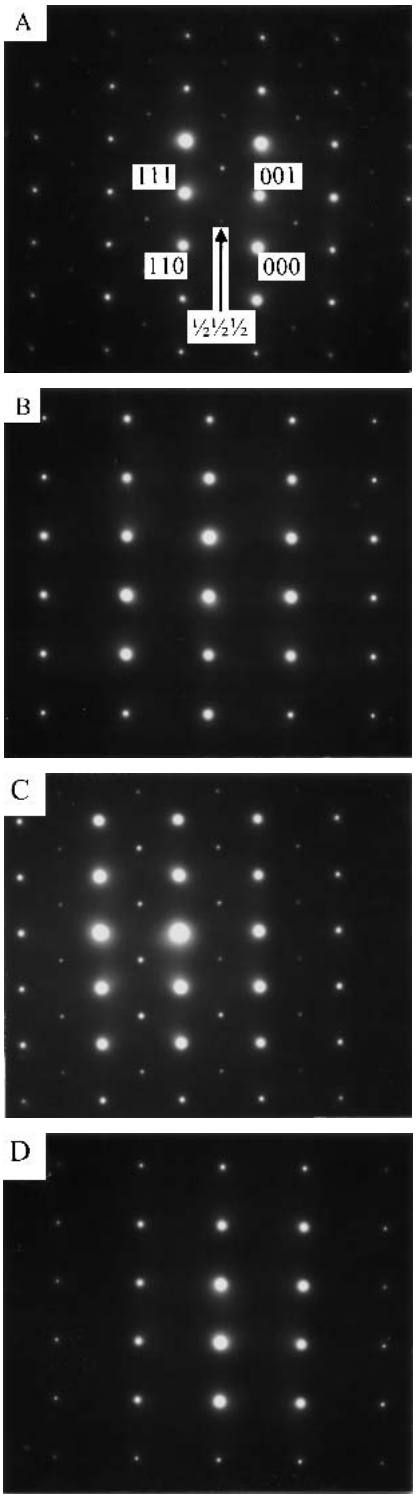

FIG. 10. $\langle 110\rangle_p$ ZADPs from the grain in Fig. 8 representing domains A–D. $\frac{1}{2}\{hkl\}_p$ superlattice reflections associated with antiphase tilting are present in domains A and C but absent in B and D.

key facts known about the appearance of $\frac{1}{2}\{hk0\}_p$ spots are the following: (i) They always occur in samples close to the AFE/FE phase boundary. (ii) They diminish monotonically in intensity as compositions plot away from the

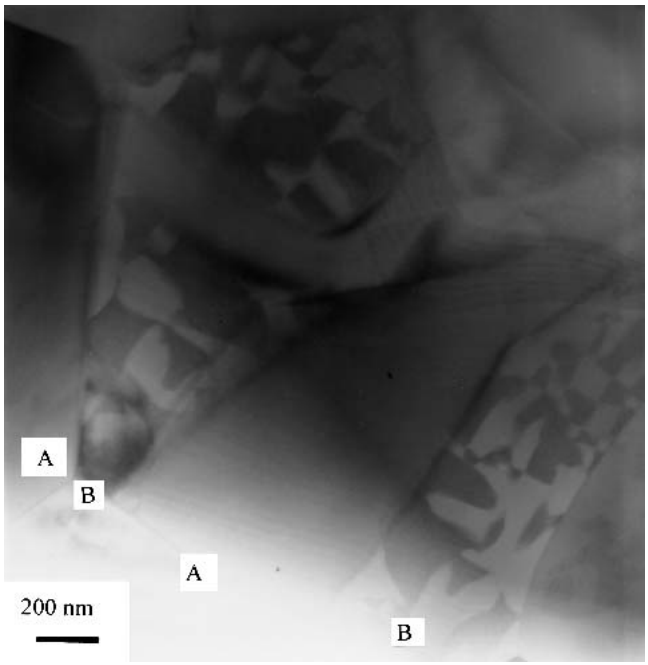

FIG. 11. BF TEM image of a PLZT 10/90/10 grain. Patchwork domain structure (B) is observed adjacent to domains free from such contrast (A).

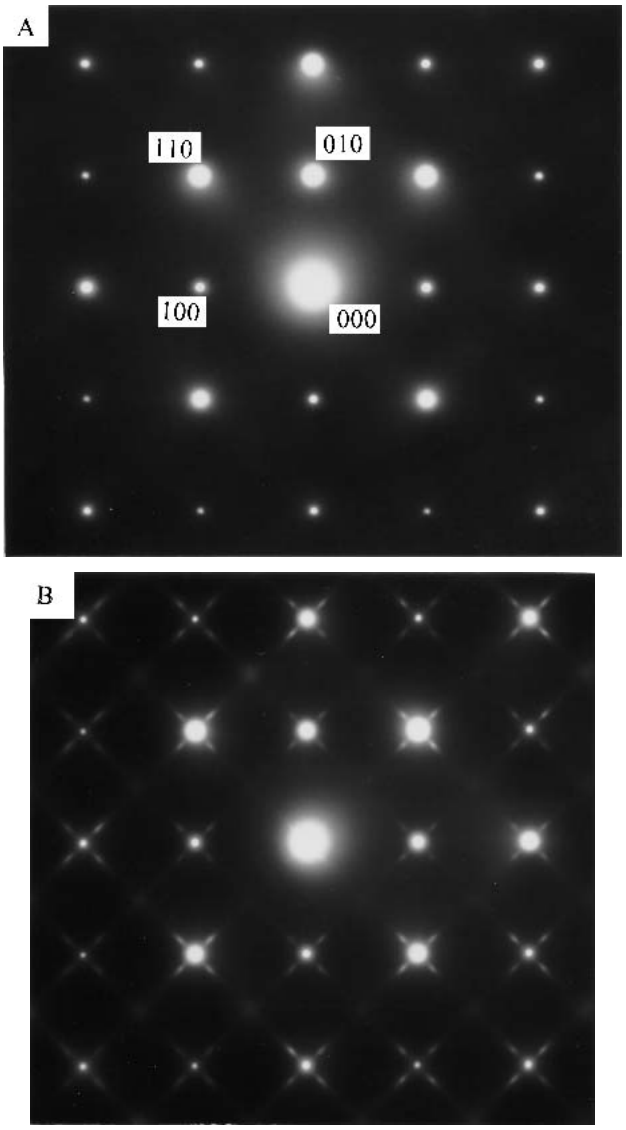

FIG. 12. $\langle 100 \rangle_p$ zone axis electron-diffraction patterns from a grain of PLZT 10/90/10 representing domains A and B, respectively, in Fig. 12. Incommensurate streaking and satellite reflections only arise from regions of the patchwork contrast.

AFE/FE phase boundary. (iii) AFE phases have $\langle 110 \rangle_p$ antiparallel displacements. (iv) FE phases near AFE/FE phase boundaries are always rhombohedral. (v) Both FE and AFE phases are tilted in antiphase. (vi) There is no x-ray/electron/neutron diffraction evidence for the presence of inphase tilting.

The following model assumes only antiphase and not inphase rotations of the octahedra and is consistent with the above facts. It is assumed that there is competition between the different distortions of the oxygen and cation sublattices associated with the AFE and FE phase in compositions close to the phase boundary. For distortions of the oxygen sublattice, it is generally accepted that the perovskite tolerance factor, t, controls the onset of octahedral rotations and is given by

$$t = R_A + R_B/\sqrt{2}(R_B + R_O) \quad ,$$

where R_A and R_B are the average A- and B-site ionic radius and R_O is the oxygen ion radius in the appropriate coordinations. In general, the AFE phase is favored if t is low. PZ has the lowest t (0.98) in the PZT solid solution which increases with the addition of PT. La substitution on the A site decreases t, since La^{3+} (1.36 Å) is smaller than Pb^{2+} (1.49 Å), thereby inducing an AFE phase in, e.g., PLZT 4/90/10. In AFE compounds, the Pb displacements in the $\langle 110 \rangle_p$ directions are coupled to antiphase rotations of the octahedra. PZ has an $a^0b^-b^-$ tilt system (PLZT 4/90/10 probably $a^0a^0c^-$) whereas an $a^-a^-a^-$ system is present in the FE rhombohedral phase according to neutron and x-ray refinements.[14,15] It is proposed that, near the phase boundary, the tilt system in the FE phase is locally $a^-b^-b^-$ where $a \approx b$. Essentially there is competition between AFE and FE phases at critical tolerance factors and $a^-b^-b^-$ represents an intermediate tilt system between $a^-a^-a^-$ (FE_R) and both $a^0b^-b^-$ (AFE_O) and $a^0a^0c^-$ ($AFE_{T/In}$). In any given region this would couple to a Pb displacement with a main component along $\langle 111 \rangle_p$ and smaller components in antiparallel along $\langle 110 \rangle_p$. Provided the regions are small (2–3 nm) and adjoining regions have components in different $\langle 110 \rangle_p$ directions, the net result would be a macroscopically averaged $\langle 111 \rangle_p$ displacement and structure. However, each nanosized region would effectively be monoclinic.

This concept is consistent with all observations and has been postulated previously by Reaney *et al.*,[18] who observed domain variance in PBZT ceramics using ½{*hk*0} reflections in a $\langle 111 \rangle_p$ zone axis at the AFE/FE phase boundary, indicating a monoclinic structure.

The most likely space group to accommodate the above structural features is *Pc*, which is a monoclinic subgroup of *R*3*c*. *Pc* has sufficient degrees of freedom on the O sites to allow antiphase rotations around all three pseudocubic axes in a manner consistent with tilt system no. 13 (listed as $a^-b^-b^-$ but represented as $a^-a^-c^-$ in the proposed structural model). Furthermore, the Pb sites allow antiparallel modulations along $\langle 110 \rangle_p$ directions of the parallel, ferroelectric $\langle 111 \rangle_p$ displacements. Simulations only provide information for one domain variant and do not imitate multidomain scattering observed in experimental diffraction patterns. Nonetheless, structural models based on *Pc* ($\sqrt{2}a_o \times \sqrt{2}a_o \times 2a_o$, where a_o is the pseudocubic lattice parameter) give rise to weak reflections in electron diffraction of the type ½{*hkl*} associated with antiphase rotations of the O octahedra along with ½{*hk*0} spots which arise when antiparallel modulations along ⟨110⟩ are applied to the ferroelectric, parallel $\langle 111 \rangle_p$ displacement, Fig. 13. If multidomain, dynamic (double diffraction) scattering is assumed, then the proposed structural model reproduces the electron-diffraction patterns obtained from the FE phase adjacent to AFE/FE phase boundary.

As La content increases ($100x = 4$), the compound becomes macroscopically tetragonal, which is accompanied by a large decrease in maximum permittivity and a change in PE behavior from classic FE to linear dielectric. Haertling and Land[3] referred to this phase as AFE_T, but electron-diffraction patterns reveal this phase to be incommensurate with a modulation along $\langle 110 \rangle_p$ directions. This phase has, therefore, been designated throughout the text as $AFE_{T/In}$. The switch from FE_R to $AFE_{T/In}$ is most likely accompanied by a change in tilt system from $a^-a^-a^-$ (or $a^-b^-b^-$ where $a \approx b$) to $a^0a^0c^-$. It is the latter tilt system that persists as La content increases ($100x = 10$), sustaining a macroscopic tetragonal distortion.

These compounds have applications as high strain transducers and large energy storage capacitors. One of the limiting criteria for the usage of AFE/FE phase change compounds is the large electrical hysteresis

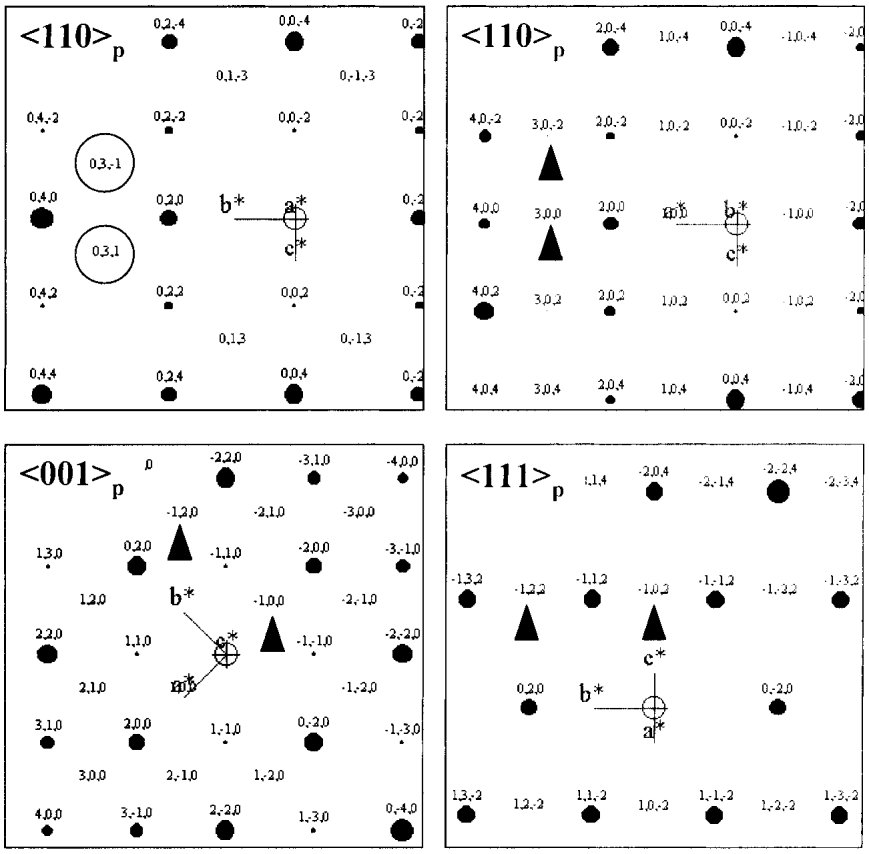

FIG. 13. Electron diffraction simulations using a structural model based on space group *Pc* of the major pseudocubic zone axes for the FE phase adjacent to the AFE/FE phase boundary. The patterns have been simulated and thus indexed using a $\sqrt{2}a_o \times \sqrt{2}a_o \times 2a_o$ unit cell whose *a* and *b* directions are at 45° to those of the pseudocubic perovsite cell but with a common *c* axis. $½\{hk0\}_p$ and $½\{hkl\}_p$ reflections are indicated by arrows and circles, respectively.

associated with switching. The phase change as a function of composition involves not only a realignment of dipoles from antiparallel (AFE) to parallel (FE) but also a change in tilt system from $a^0a^0c^-$ to $a^-a^-a^-$ (or $a^-b^-b^-$, $a \approx b$) It is postulated that the changes in structure induced by variation in x are equivalent to those induced by a strong electric field. It is expected therefore that electrical switching in e.g., PLZT 4/90/10 from AFE to FE will require an O-octahedral network as well as dipolar rearrangement. The activation energy associated with this change may be responsible for the large electrical hysteresis observed in these systems. The large hysteresis may therefore be intrinsic to the phase change.

V. CONCLUSIONS

(1) XRD and electrical measurements show an AFE/FE phase change between PLZT 2/90/10 and PLZT 4/90/10, in agreement with the authors of Ref. 3. The sequence of line splitting suggests a tetragonal structure, but electron diffraction clearly shows the appearance of an incommensurate AFE modulation in most grains of PLZT 4/90/10, consistent with work reported by the authors of Refs. 4 and 8.

(2) The domain structure of PLZT 2/90/10 (FE) is complicated due to the proximity of the AFE phase boundary. FE regions exhibit a modulated domain contrast adjacent to $AFE_{T/In}$ regions in the same grain.

(3) $\frac{1}{2}(hk0)$ reflections are observed in electron-diffraction patterns in the FE phase immediately adjacent to the AFE/FE phase boundary. These do not arise from in-phase tilting but from Pb displacements coupled to an $a^-b^-b^-$ ($a \approx b$) tilt system present immediately adjacent to the AFE/FE phase boundary. A structural model based on the space group Pc has been proposed to explain all the observed superlattice reflections.

(4) PLZT 4/90/10 shows systematic absences of the $\frac{1}{2}\{hkl\}_p$ superlattice reflections in alternate $\langle 110\rangle_p$ domains in addition to a tetragonal distortion, consistent with an $a^0a^0c^-$ tilt system. This tilt system sustains a tetragonal distortion even though the long-range antipolar AFE coupling diminishes as La content increases.

(5) In PLZT 4/90/10 and 10/90/10, domain variance of the incommensurate modulation is observed with only alternate domains giving rise to satellite reflections. Domains that exhibit incommensurate spots often exhibit a complex patchwork contrast.

ACKNOWLEDGMENTS

This work was carried out as part of Technology Group 01 of the MoD Corporate Research Programme. The authors thank Dr. D. Hall at the Materials Science Centre, University of Manchester, Manchester, U.K., for allowing use of his PE field equipment.

REFERENCES

1. D. Berlincourt, IEEE Trans. Sonics Ultrason. **SU-13,** 116 (1966).
2. K.G. Brooks, J. Chen, K.R. Udayakumar, and L.E. Cross, J. Appl. Phys. **75,** 1699 (1994).
3. G.H. Haertling and C.E. Land, J. Am. Ceram. Soc. **54,** 1 (1971).
4. X. Dai and D. Viehland, J. Appl. Phys. **76,** 3701 (1994).
5. G. Shirane, K. Suzuki, and A. Takeda, J. Phys. Soc. Jpn. **7,** 12 (1952).
6. G. Shirane, Phys. Rev. **86,** 219 (1952).
7. G. Shirane and S. Hoshino, Acta Crystallogr. **7,** 203 (1954).
8. Z. Xu, D. Viehland, P. Yang, and D.A. Payne, J. Appl. Phys. **74,** 3406 (1993).
9. Z. Xu, Z. Dai, and D. Viehland, Appl. Phys. Lett. **65,** 3287 (1994).
10. Z. Xu, Z. Dai, and D. Viehland, Phys. Rev. B **51,** 6261 (1995).
11. X. Dai, Z. Xu, and D. Viehland, J. Appl. Phys. **77,** 5086 (1995).
12. X. Dai, Z. Xu, and D. Viehland, J. Am. Ceram. Soc. **78,** 2815 (1995).
13. Z. Xu, X. Dai, J.F. Li, and D. Viehland, Appl. Phys. Lett. **66,** 2963 (1995).
14. J. Ricote, D.L. Corker, R.W. Whatmore, S.A. Impey, A.M. Glazer, J. Dec, and K. Roleder, J. Phys. Condens. Matter. **10,** 1767 (1998).
15. A.M. Glazer, Acta Crystallogr. B **28,** 3384 (1972).
16. A.M. Glazer, Acta Crystallogr. A **31,** 756 (1975).
17. A.M. Glazer, S.A. Mabud, and R. Clarke, Acta Crystallogr. B **34,** 1060 (1978).
18. I.M. Reaney, A. Galzounov, F. Chu, A. Bell, and N. Setter, Br. Ceram. Trans. **96,** 217 (1997).
19. S. Watanabe and Y. Koyama, Phys. Rev. B **63,** 134103-1 (2001).
20. H.F. Kay and P.C. Bailey, Acta Crystallogr. **10,** 219 (1957).
21. I.M. Reaney, Proc. Electroceram. V **1,** 441 (1996).
22. C.A. Randall, D.J. Barber, R.W. Whatmore, and P. Groves, J. Mater. Sci. **21,** 4456 (1986).
23. D.L. Corker, A.M. Glazer, J. Dec, K. Roleder, and R.W. Whatmore, Acta Crystallogr. B **53,** 135 (1997).